TRENDS IN SCIENCES 2026; 23(2): 11206
https://doi.org/10.48048/tis.2026.11206 RESEARCH ARTICLE

Synthesis and Corrosion Protection of 3:1 MgAl Layered Double Hydroxides: Metals Concentration Study via Coprecipitation

Mohamad Nor Amirul Azhar Kamis[1], Hamizah Mohd Zaki[1,2,*], Adila Mohamad Jaafar[4], Mohammad Noor Jalil[1,3] and Nur Shafiqa Nabila Mohd Nor[1]

[1]*Faculty of Applied Sciences, Universiti Teknologi MARA, Shah Alam, Selangor 40450, Malaysia*
[2]*Multifunctional Nanoporous Material Research (MULNA), Universiti Teknologi MARA, Shah Alam, Selangor 40450, Malaysia*
[3]*Electrochemical Material and Sensor (EMaS), Universiti Teknologi MARA, Shah Alam, Selangor 40450, Malaysia*
[4]*Materials Synthesis and Characterization Laboratory, Institute of Advanced Technology, Universiti Putra Malaysia, Serdang, Selangor 43400, Malaysia*

([*]Corresponding author's e-mail: hamiz410@uitm.edu.my)

Received: 7 July 2025, Revised: 29 July 2025, Accepted: 5 August 2025, Published: 1 November 2025

Abstract

This study investigates the effect of metal ion concentration on the formation and properties of Mg-Al Layered Double Hydroxides (LDHs) with a fixed Mg^{2+}/Al^{3+} molar ratio of 3:1. While previous studies often report this ratio, the influence of concentration on LDH purity and structure remains less explored. LDH samples synthesized through coprecipitation method at varying concentrations were characterized using PXRD, TGA, FTIR, FESEM, BET surface area analysis, and elemental analysis techniques. The findings confirm the successful formation of nitrate-intercalated LDHs across all concentrations, with consistent structural and morphological features. Although metal concentration influenced the crystallinity and surface characteristics, the highest metal concentration LDH (S3) was observed to efficiently inhibit the corrosion of mild steel in neutral NaCl solution through ion-exchange process.

Keywords: Layered Double Hydroxide (LDH), Optimization, Corrosion inhibition, Synthesis, Concentration variations, Mild steel, Electrochemical measurement

Introduction

The Layered Double Hydroxide (LDH) structure consists of 2 components: Positively charged metal layers and an intermediate layer consisting of water molecules and adsorbed anions embedded between the metal layers. LDH has a general formula of $(M^{2+}_{1-x}M^{3+}_{x}(OH)_2)^{x+}(A^{n-}_{x/n}\ yH_2O)^{x-}$ where M^{2+}, M^{3+} is the divalent and trivalent cations, respectively. The x is the molar ratio of divalent to trivalent cations in the metal layers, generally between 2.0 - 6.0 [1]. A^{n-} is the adsorbed anion in the metal interlayer to stabilize the LDH structure. The adsorbed anions can be replaced via an anion exchange process based on the affinity of the anion towards the LDH structure. The planarity of the anion also plays an important role in anion exchange due to the flat plane of the LDH structure. Carbonate and nitrate are the favored anions due to their trigonal planar molecular geometry which easily fits into the LDH structure. The anion exchange process can be readily conducted with anions that have lower adsorption affinity, such as nitrate, in comparison to carbonate, which has a higher affinity towards LDH structure. Other common anions used in the formation of LDH follow the order of anion affinity strength; $CO_3^{2-} > SO_4^{2-} > OH^- > F^- > Cl^- > Br^- > NO_3^- > I^-$ [2,3]. The general equation of anion exchange action that takes place within the LDH structure is presented in Eq. (1);

$$LDH\text{-}A + B^- \rightarrow LDH\text{-}B + A^- \quad (1)$$

where A is the anion primarily from the LDH, and B is the foreign anion with higher affinity towards the LDH structure. From the anion exchange mechanism, the amount of the foreign anion can be reduced from the target mixture/material due to entrapment in the interlayer. The primary anion released can be used as a catalyst or inhibitor for designated features.

LDH has a wide range of applications, including the production and processing of polymers, catalysis, sorption and decontamination processes for the intercalation of various substances. LDH is a potentially good adsorbent due to low cost, ease of preparation, highly effective, high chemical stability and environmental safety [4]. Due to the sustainability of LDH, it is also applied to corrosion inhibition for neutral and alkaline systems [5].

There are several methods used to synthesis the LDH such as coprecipitation, hydrolysis, combustion, and sol-gel method. Among all, the most commonly used synthesis method to form the LDH is the coprecipitation method, where 2 metal salts are reprecipitated in an alkaline solution at a constant pH value.

MgAl LDH is a promising layered material often regarded as a 'green material' [4] and is widely used in environmental protection research. The ideal pH for synthesizing MgAl LDH is approximately 10 [6]. This pH promotes the formation of a well-ordered structured LDH. Higher alkaline pH values would produce low-purity LDH with the presence of metal oxides.

Previous research on the synthesis of layered double hydroxides (LDH) has emphasized the molar ratios of the metals used, at a 3:1 ratio of magnesium to aluminium. Other studies have also investigated the effect of ageing time and temperature [7], and the amount of the precipitating agent, NaOH [8], revealed different morphology of the synthesized LDH. However, no study has been conducted on the optimal concentrations of these metals required to attain sufficient purity for anion exchange properties. Thus, this study aims to investigate the effect of varying the concentration of metal salts used in the synthesis of magnesium-aluminium nitrate ($MgAl\text{-}NO_3^-$) LDH, while maintaining a fixed molar ratio of 3:1 (Mg to Al) through a coprecipitation method.

The properties of the synthesized LDH were thoroughly analyzed to assess how these concentration variations influence the characteristics of LDH. Herein, the characteristics of the synthesized LDH was evaluated for corrosion protection against mild steel, which is widely used in industrial applications. The corrosion study was carried out in a neutral NaCl (3.5 wt%) solution. The anticipated reaction with the addition of LDH into NaCl solution as the following chemical equation (Eq. (2));

$$LDH\text{-}NO_3^- + NaCl \rightarrow LDH\text{-}Cl^- + NaNO_3 \quad (2)$$

The reaction occurs due to the ability of LDH structure to perform the anion exchange, where, in this case, the chloride has higher anion affinity compared to nitrate towards the layered structure of LDH. The $NaNO_3$ will be the side product that is a soluble salt which is non-hazardous to the environment [9].

Materials and methods

Materials

$Mg(NO_3)_2.6H_2O$ (99%, Merck), $Al(NO_3)_3.9H_2O$ (98.5%, R&M Chemicals), NaOH (99%, Merck) were used for synthesis without further purification. Deionized water was used throughout the synthesis wherever required to prevent the interference of carbonate. NaCl (99.5%, R&M Chemicals) was utilized in the corrosion protection study via electrochemical analysis.

Synthesis of $MgAl\text{-}NO_3^-$ layered double hydroxides via coprecipitation method

Three Mg-Al LDH samples were synthesized using a molar ratio of 3:1 with concentrations of 0.03M:0.01M (S1), 0.06M:0.02M (S2), and 0.09M:0.03M (S3). The mass used was calculated based on 50 mL of deionized water. The mixture was vigorously stirred (500 rpm) at room temperature to ensure homogeneity. The pH value was controlled at 10 ± 0.3 by adding NaOH (2M) dropwise while introducing N_2 to avoid carbonate interference. The precipitate was recovered by centrifugation (4,000 rpm for 10 min), washed with deionized water and repeated 3 times.

The sample was then dried in an oven at 90 °C overnight. **Scheme 1** illustrates the procedure used in synthesizing the LDH used in this study.

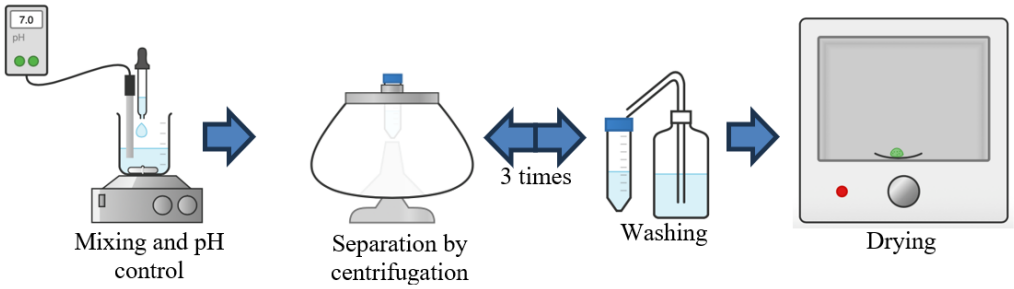

Scheme 1 Representation of the preparation process for MgAl LDH.

Characterization of MgAl-NO_3^- LDH

The powder X-ray diffraction patterns of the prepared LDH were analyzed on a PANalytical X'pert PRO, 45 kV, 40 mA with 2θ range of 5° - 80° and scan speed of 2°/min. Fourier transform infrared (FTIR) spectra using KBr pellet method were recorded on a Perkin Elmer Spectrum 1725X within the range of 450 - 4,000 cm^{-1}. The thermal analysis of the samples was determined using a Netzsch Thermogravimetric Analyzer (USA) with a heating rate of 10 °C/min within the range of 30 - 1,000 °C under a nitrogen atmosphere. The composition of each sample was analyzed using a CHNS Analyzer 2400 PerkinElmer Series II (USA) with dynamic flash combustion technique. The surface morphology of the samples was characterized using a Field Emission Scanning Electron Microscope (FESEM), Carl Zeiss Supra 40 (USA) at 100k magnification. The surface area and porosity of the samples were determined using a Micromeritics ASAP 2060 (USA) with nitrogen gas adsorption-desorption at 77K with prior degassing in an evacuated-heated chamber at 120 °C for 8 h.

Electrochemical analysis for corrosion protection of mild steel

The test solution used in this study was the neutral 3.5 wt% of NaCl without and with LDH (100 ppm). Electrochemical measurements were performed using a Metrohm Autolab Potentiostat Galvanostat AUT86669 (Netherlands). A 3-electrode cell was used with a platinum rod as the auxiliary electrode (AE), an Ag/AgCl electrode as the reference electrode (RE), and mild steel as the working electrode (WE) with an exposed area of 0.1 cm^2. A schematic representation of the 3-electrode setup used in the electrochemical measurements is shown in **Scheme 2**.

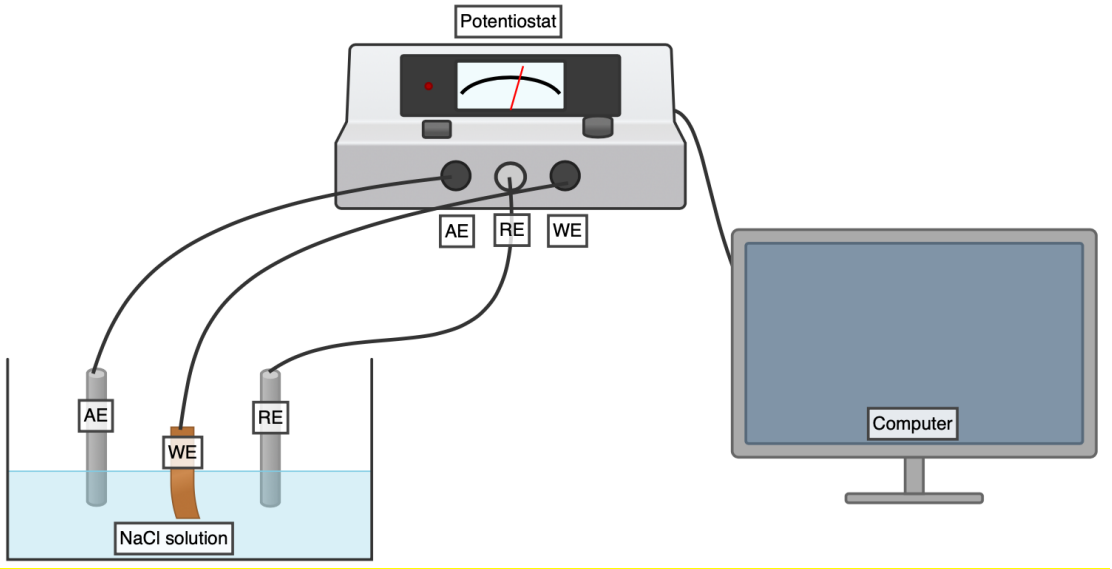

Scheme 2 Schematic illustration of the electrochemical analysis experiments using the 3-electrode system.

The electrochemical impedance measurements were performed over a frequency range of 100 kHz to 100 mHz with 7 points per decade using 5 mV and peak-to-peak sinusoidal voltage. Anodic and cathodic polarization curves, in the absence and presence of LDH were obtained with a scan rate of 1 mV/s over the open circuit potential. Corrosion potentials (E_{corr}) of anodic and cathodic curves were extrapolated to obtain the corrosion current density (I_{corr}) values. The inhibition efficiency (η) was calculated using Eq. (3);

$$\eta = 1 - \frac{i_{corr(i)}}{i_{corr(0)}} \quad (3)$$

where $i_{corr(i)}$ and $i_{corr(0)}$ are the current density of mild steel in the NaCl solution with and without the presence of LDH, respectively [9].

Results and discussion

Physicochemical characterization of MgAl LDH

The X-ray diffraction patterns of synthesized MgAl LDH shown in **Figure 1** examine the crystal structure of the material. All samples show the characteristic of layered materials with relatively intense sharp reflection peaks at lower 2θ values and less intense reflection peaks at higher 2θ.

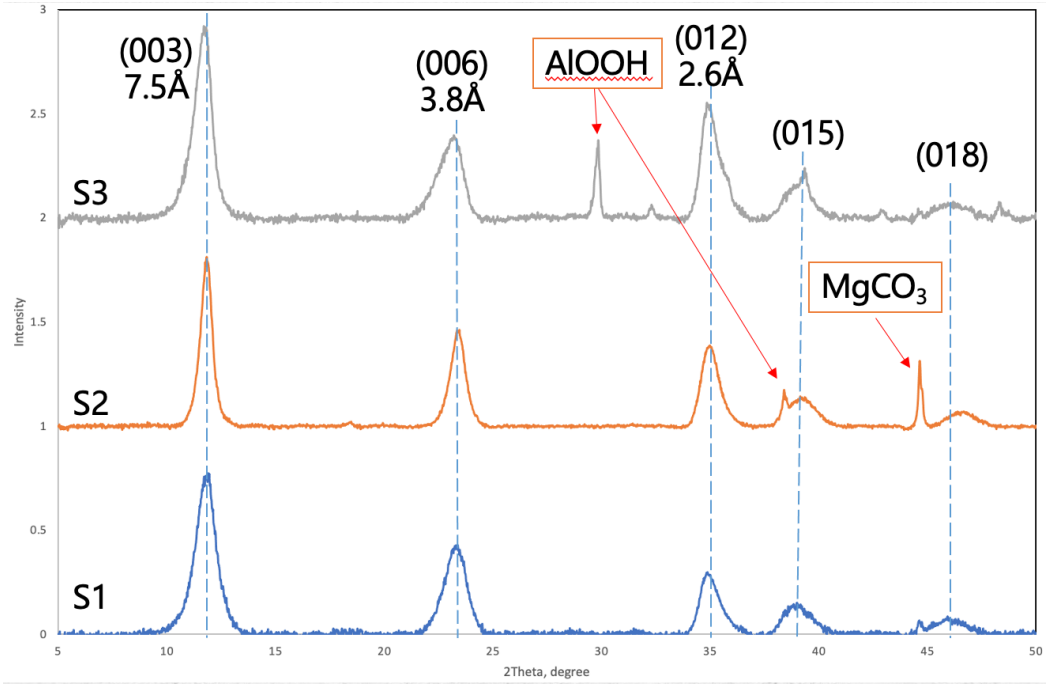

Figure 1 PXRD patterns of 3:1 MgAl-NO_3^- LDHs with different M^{2+}/M^{3+} concentrations.

All samples exhibit the typical character of the layered compound with the presence of (003), (006) and (012) reflections with a basal spacing of 7.5, 3.8 and 2.6 Å, respectively [10]. These reflection peaks indicate the formation of the typical layered structure of MgAl-LDHs, which most likely have a similar anion orientation within the interlayer galleries. The highest intensity reflection peak of (003) at 2θ = 11.79° confirms the presence of water and hydroxide layer, which are parts of the LDH compounds [11]. The basal spacing of the reflection peaks obtained by using Bragg's law (Eq. (4));

$$\lambda = 2d \sin \theta \quad (4)$$

where λ is the wavelength used to obtain the diffraction pattern of 1.5406 Å, d is the basal spacing, and θ is the angle of the diffraction peak, respectively [9].

At lower metal concentrations, S1 shows pure LDH phase form where all diffraction peaks only correspond to the MgAl-NO_3^- LDH. S2 with the molar concentration of 0.06M:0.03M (Mg:Al) shows the presence of $MgCO_3$ peak around 2θ = 45° due to the incomplete reaction of Mg with Al to form the metal layers. The higher metal concentration used in S3 shows the additional peak of boehmite, AlOOH [12], around 2θ = 28°, which may also be due to the incomplete reaction of Al. Moreover, a longer ageing period and slower synthesis rate might avoid these unnecessary products to ensure a complete reaction between the metals [7].

The formation of different crystal phases was observed to have an impact on the degree of crystallinity of the sample. In order to evaluate the crystallinity of the samples, the full width half maximum (FWHM) value was calculated using X'Pert Highscore software [13], as presented in **Table 1**. Among the samples prepared, S2 has the highest crystallinity with lowest FWHM value. It can be observed based on the shape of the diffraction peak of S2; sharper and more symmetric. Other samples show slightly higher FWHM indicating low crystallinity with higher anion exchange capability [14]. Broader reflection peaks indicate that the LDH formed probably in the amorphous phase where the atoms are arranged irregularly.

Table 1 Assessment of LDH crystallinity by full width half maximum.

	FWHM
S1	1.137 ± 0.02
S2	0.671 ± 0.01
S3	0.993 ± 0.02

Elemental analysis data executed from FESEM with the EDX method for the synthesized LDHs are summarized in **Table 2**. Theoretical values of the metal content were calculated using LDH formula of $Mg_3Al(OH)_2NO_3.2H_2O$. S1, with the lowest metal concentration, shows the closest to the theoretical values showing the high-purity product. **Figure 2** shows the EDX spectrum of S1 with the presence of respective elements. Other samples (S2 and S3) show deviation of the metals content from theoretical values, which might be explained by side products other than LDH phases as discussed in the PXRD section.

Table 2 Elemental analysis data for MgAl LDHs with different metal concentrations analyzed using FESEM-EDX method. The theoretical weight percent of Mg and Al calculated based on the general molecular formula of LDH were 31.44% and 11.64%, respectively.

	Content, wt%			
	Mg	**Al**	**Mg:Al**	**N**
S1	30.32	10.65	2.8:1	1.01
S2	25.59	10.77	2.4:1	1.12
S3	20.56	7.09	2.9:1	1.35

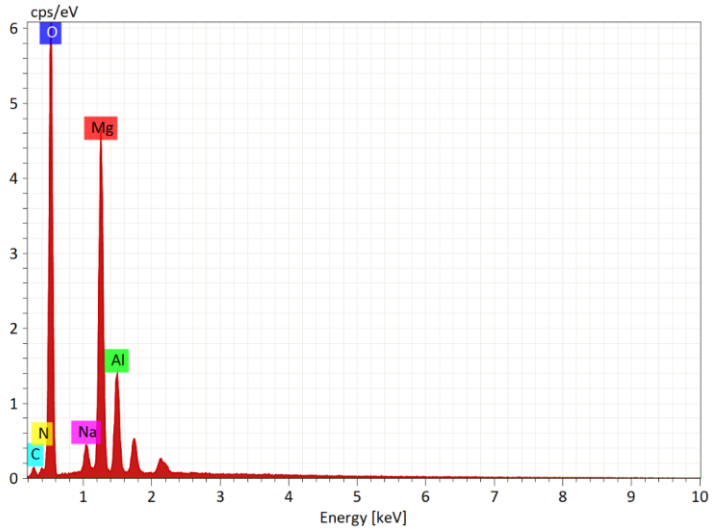

Figure 2 FESEM EDX spectrum of S1 showing the presence of elements in the synthesized LDH.

The M^{2+} to M^{3+} ratio is in agreement with the theoretical value considering the proportions of metals used in the synthesis. The intercalation of nitrate is proven and supports the result from the elemental analysis through CHNS analyzer.

The amount of intercalated anion, nitrate was determined using the CHNS Analyzer, presented in **Table 3**. The result shows that S3, with the highest metal concentration used, formed the layered structure with the highest amount of intercalated nitrate due to the highest value of N content in the sample. The interference of carbonate in the interlayer was observed to be the lowest in S1 based on the C content. This signifies that the lowest metal concentration used is able to refrain the unwanted carbonate in the interlayer. The H content for all samples is around 3.4% showing that

the similar amount of interlayer adsorbed water and the hydroxyl group on the metal layers.

Table 3 Weight contents of C, H and N elements in different samples analyzed using CHNS analyzer.

	S1	S2	S3
Carbon (%)	1.48	2.60	2.75
Hydrogen (%)	3.34	3.44	3.48
Nitrogen (%)	1.06	1.29	2.33

The molecular bonding for the synthesized LDHs analyzed using FTIR technique with KBr pellet is presented in **Figure 3**.

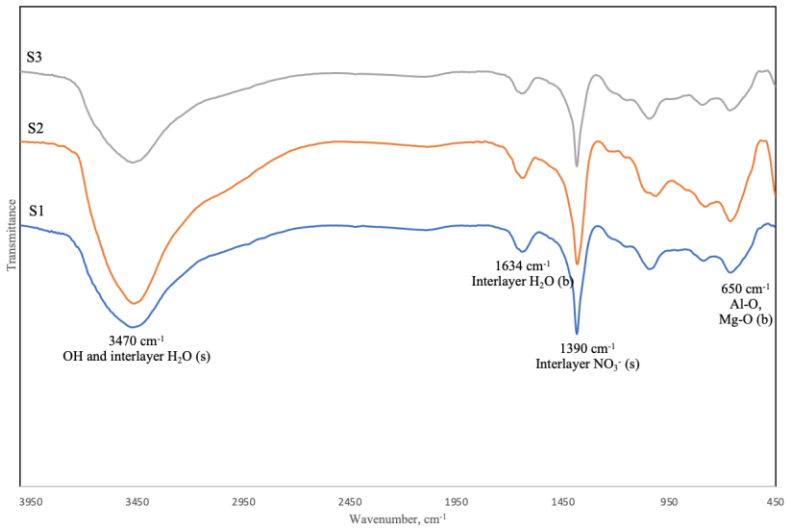

Figure 3 FTIR spectrum of MgAl-NO_3^- LDHs with different M^{2+}/M^{3+} concentrations.

All samples show most likely similar vibration peaks. The region in between 460 - 1,000 cm^{-1} shows the region of vibration peaks correspond to the metal oxide; MgO and Al_2O_3 [10,15-18]. The absorption band observed at 650 cm^{-1} is due to the presence of Al-O and Mg-O groups in the layer [19]. It is noticeable difference at S2 with sharpest peak at 650 cm^{-1} due to high crystallinity based on the calculated FWHM values from the PXRD patterns. The broad peak observed around 3,490 cm^{-1} is attributed to the physically adsorbed water molecules and the hydroxyl groups on LDH surface [16,17,20]. The bending vibration of the interlayer water molecules is observed around 1,660 - 1,670 cm^{-1} [15,21]. The intercalated nitrate between the metal layers is observed at 1,390 cm^{-1} [15,16] in all spectrums, indicating the presence of nitrate as a counter ion to balance the LDH structure. A weak band observed around 1,088 cm^{-1} in all samples corresponds to the in-plane vibration of carbonate ions, which is unavoidable due to the interference of atmospheric CO_2 during synthesis and drying processes.

Thermal behavior of the synthesized LDHs were investigated using TG and DTG techniques at room temperature up to 1,000 °C presented in **Figure 4**. Three steps of degradation behaviour were observed in all samples corresponding to the interlayer and surface water dehydration, dehydroxylation of hydroxide layers and decomposing anion, and rupturing of the residual metal layers, respectively [20,22].

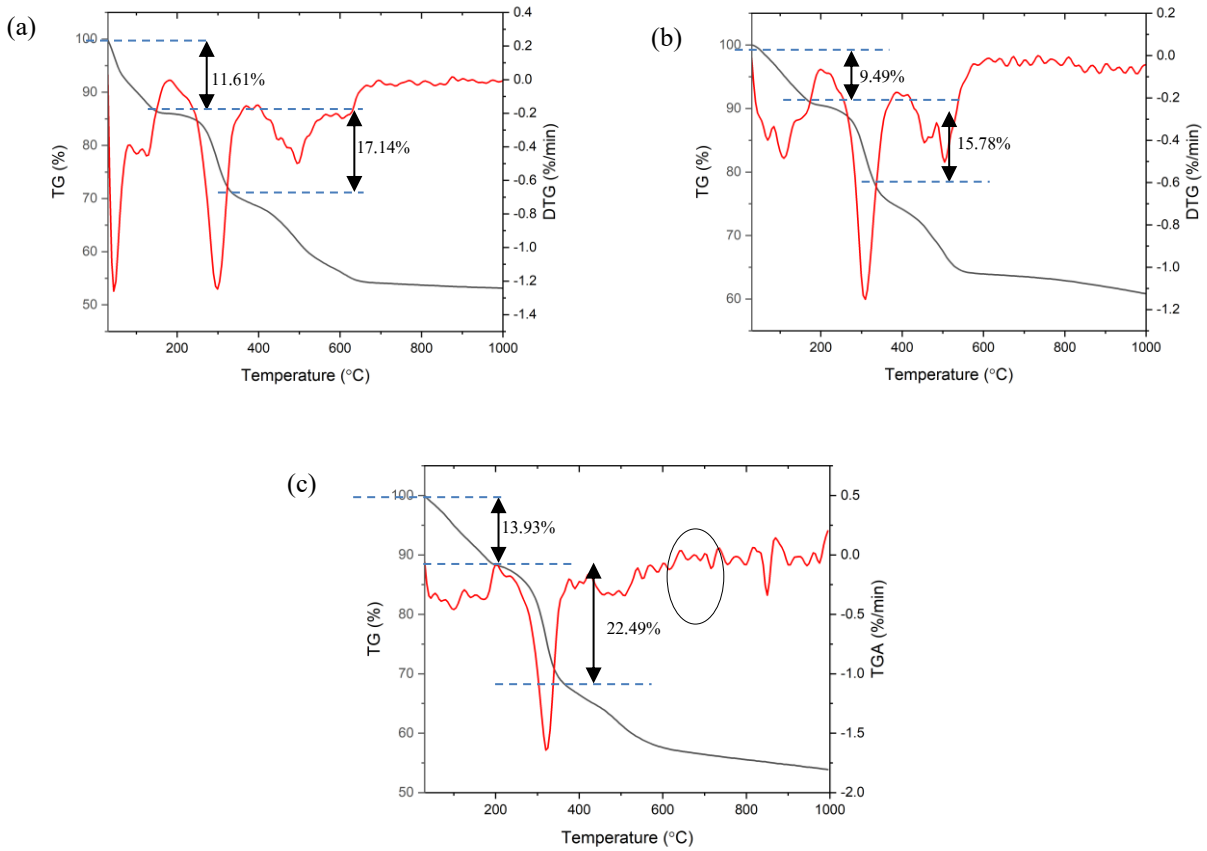

Figure 4 TG/DTG curves of (a) S1, (b) S2, and (c) S3.

The 1st decomposition of water in the compounds reveal the different amount of adsorbed water [17,18,23] of LDHs; 11.61%, 9.49% and 13.93% of weight losses for S1, S2 and S3 respectively (**Figure 4**). At this stage, the LDH turns into an anhydrous compound where the reaction follows Eq. (5). The water adsorbed in the interlayer is used to balance the structure with regard towards the amount of nitrate. Since S3 is characterized with highest amount of nitrate, in CHNS result, it is concurrent result with the highest amount of adsorbed water, corresponds to the 13.93%.

$$MgAl\text{-}NO_3^-.xH_2O(OH)\ LDH \rightarrow MgAl\text{-}NO_3^-(OH)\ LDH + xH_2O\ (gas) \quad (5)$$

The 2nd decomposition temperature of the anion [15,20,24] and the dehydoxylation of hydroxide layer starts at 450 °C (17.14%), 433 °C (15.78%) and 438 °C (22.49%) for S1, S2 and S3 respectively. The results show that S3 has highest amount of intercalated nitrate as supported by the elemental analysis analyzed by CHNS Analyzer. The reactions occurred in the 2nd decomposition stage for dehydroxylation of hydroxide layer, and decomposition of intercalated nitrate are given in Eqs. (6) and (7) respectively;

$$MgAl\text{-}NO_3^-(OH)\ LDH \rightarrow MgAl\text{-}NO_3^-\text{-}Oxide\ LDH\ (unstable) + H_2O\ (gas) \quad (6)$$

$$NO_3^- \rightarrow NO_x + O_2\ (gas) \quad (7)$$

The residue of non-volatile metals obtained after the complete decomposition was approximately 57 ± 4 wt%. The reaction for the decomposition of LDH into metal oxides is given in Eq. (8);

$$MgAl\text{-}Oxide\ LDH\ (unstable) \rightarrow MgO + Al_2O_3 \quad (8)$$

The endothermic behavior observed above 600 °C is due to the further decomposition of residual interlayer anions and crystallization of oxide mixtures such as $MgAl_2O_4$ [20]. An additional endothermic curve was

only detected in S3 at 830 °C due to the presence of impurities, supports the previously discussed data.

The specific surface area and pore-size distribution of the synthesized LDH were studied from N_2 adsorption-desorption plots and Barret-Joyner-Halenda (BJH) curve. The physisorption isotherms of the LDH measured at 77K are shown in **Figure 5**.

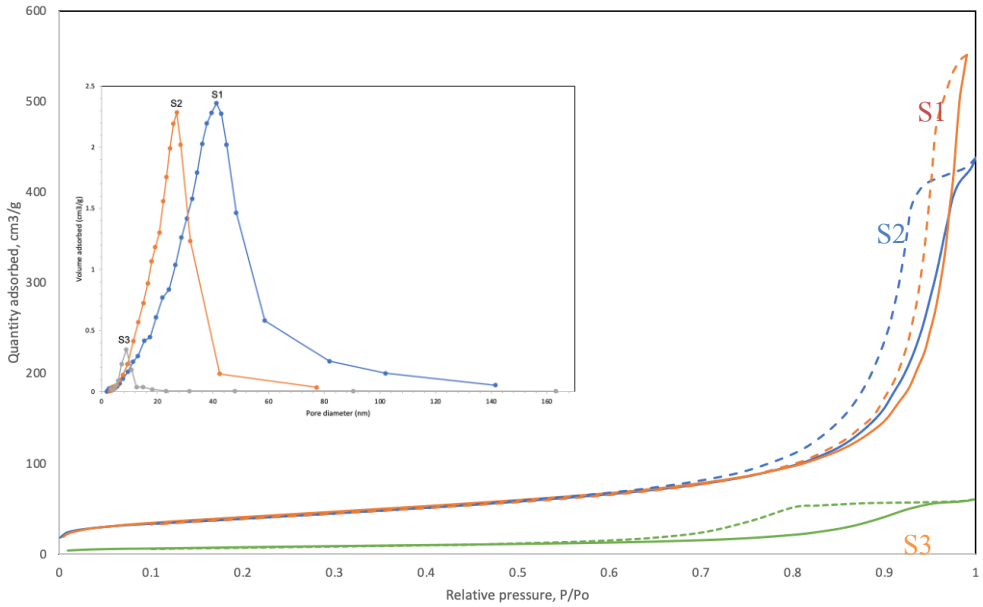

Figure 5 Nitrogen adsorption-desorption isotherms with the inset shows the BJH plot for pore size distribution of the synthesized LDH. Solid line refers to the adsorption and dotted line refers the desorption of nitrogen gas.

All samples displayed a type IV isotherm where S1 and S2 have sharp uptakes with S1 adsorbs more than 500 cm^3 N_2 gas for each gram of sample, while S2 only adsorb around 420 cm^3/g. The mechanism of desorption of these 2 samples also different where S2 needs extra pressure different in the beginning of the desorption process compared to S1. This might be due the different pore shape which cause the difficulty of N_2 to leave the pore. High surface adhesion is another factor causing the difficulty of N_2 to desorb from the surface.

S1 isotherm was observed to possess the H_3 hysteresis loop with no limiting adsorption at high P/P_o attributed to parallel shape pore, while S2 isotherm shows an H_1 hysteresis loop portraying the cylindrical shape pore. In contrast, S3 shows the lowest adsorption-desorption isotherm with H_2 hysteresis loop ascribed the ink-bottle shape pore. The difference in the hysteresis loop can also be explained by the different stacking on the layers in the crystal [25], as observed in FESEM micrographs. The presence of interferences observed in PXRD impacts the surface area of the LDH, where S3 is only able to adsorb less than 100 cm^3 of N_2 gas for each gram. The reduction of the surface area and pore volume of S3 in **Table 4** are due to the high amount of intercalated ion in the metal layer, which will be extensively used in the anion exchange process [26].

Table 4 BET surface area and average pore diameter of MgAl LDHs synthesized with different metal concentrations.

	S1	**S2**	**S3**
BET surface area, m^2/g	147.79	140.27	28.74
Average pore diameter, nm	24.62	17.43	7.79

Based on the isotherms and average pore diameter values, it is validated that all samples are formed with Type IV mesoporous structure with pore size between 2 - 50 nm [27]. The average pore diameter of all samples was larger than the size of the nitrate ion (0.33 nm), which enables the reduction of the physical barrier effect for ions to encapsulate the pore channels, hence being more beneficial for adsorption [25].

The morphology of the synthesized LDHs observed by FESEM shows a slight difference in particle size and shape, as shown in **Figure 6**. All samples exhibit the typical morphology of layered compounds with aggregated plate-like shapes. The formation of LDH morphology is due to the hydroxide group regulating the oriented growth for the layered structure [16]. S1, with the lowest metal concentration, shows a very fine plate-like shape, which produces high porosity and high surface area, confirmed by nitrogen adsorption-desorption isotherm. The irregular stack of the nanosheet material with the convex and concave fold forms the mesoporous structure of S1 LDH [25]. It was reported in another study that the amount of NaOH used in the LDH preparation also affected the shapes of LDH [8]. Different shape materials affect the porosity of material which portrayed by the surface area. A highly porous structure helps to improve the adhesion onto the surface and is able to provide numerous active sites for chemical and physical interaction.

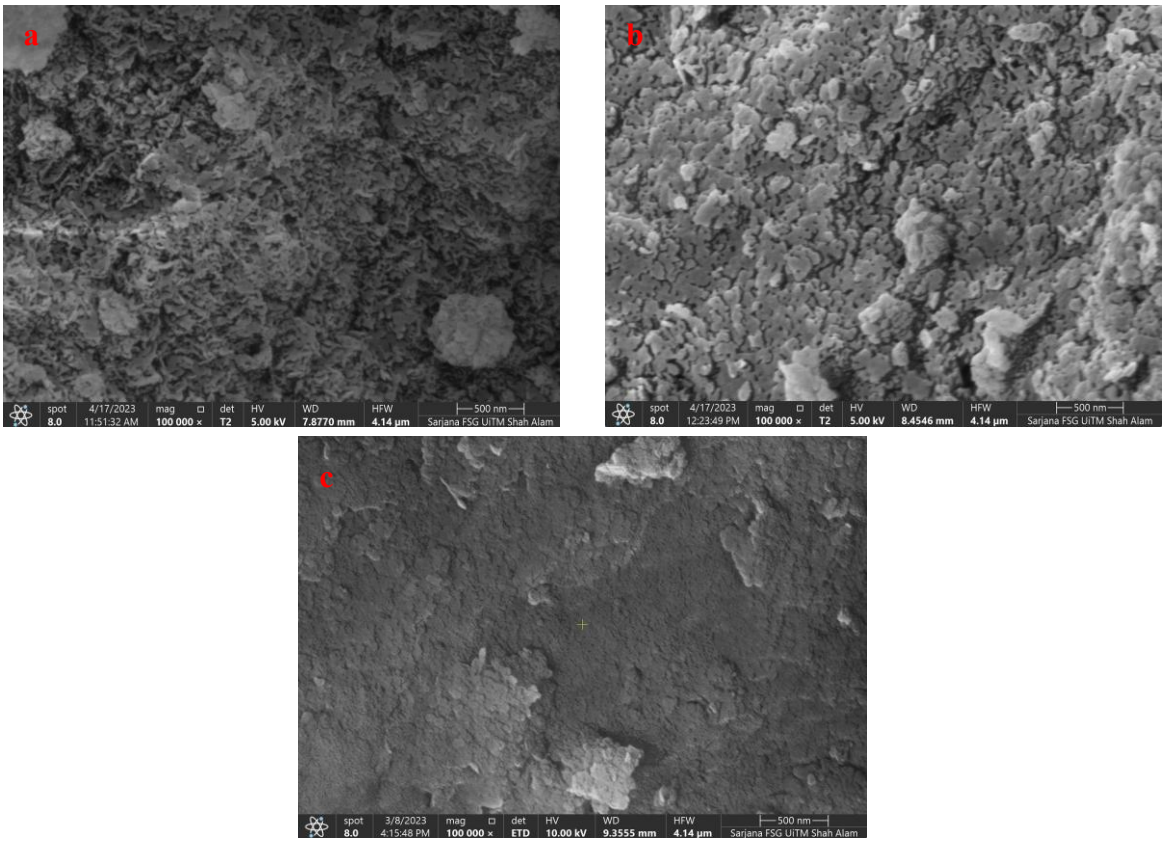

Figure 6 FESEM micrographs of (a) S1, (b) S2, and (c) S3 at 100K magnification.

The typical plate-like structure of LDH with a mean size of 30 nm was observed in S2 and has poor adhesion onto the surface, making it difficult to apply as a coating [28]. The morphology also shows lower porosity which has fewer voids to provide anchoring points for coating. In contrast, S3 shows a nonporous surface where particle agglomeration and swelling are observed due to a high concentration of nitrate between the metal layers, resulting in a smaller gap between the particles [24,29]. It was validated with the value of the small BET surface area of S3 compared to S1 and S2, tabulated in **Table 4**. This phenomenon might be due to the rapid growth of particles under alkaline oversaturation conditions [20].

In spite lower ability of S3 to adhere on the metal surface compared to S1 and S2, it was confirmed that it has the highest amount of nitrate to be used as corrosion inhibitor. Since the mechanism of corrosion inhibition is due to the anion exchange, it is anticipated that S3 will have the highest inhibition efficiency with high amount of nitrate to be adsorbed on the metal surface. The nitrate will form the protecting layer which repel the corrosive chloride in the test solution [9].

Corrosion inhibition performance

The ability of the synthesized LDH to inhibit corrosion by the presence of nitrate was evaluated using electrochemical impedance spectroscopy (EIS). The Nyquist plot of mild steel in neutral 3.5 wt% NaCl solution with and without LDH is presented in **Figure 7(a)**. The presence of LDH in the test solutions shows the formation of 2 capacitive impedance arcs with a bigger capacitive arc radius, indicating improvement in corrosion resistance [17]. The 2nd capacitive arc at a lower frequency was due to the formation of a protective layer from the inhibitor (nitrate) from the LDH structure to resist the corrosive chloride in the solution. S1 and S2 show comparable pattern and size of capacitive loop, which anticipated to have a slight difference in the corrosion inhibition efficiency. In S3, the size of the 2nd capacitive loop is significantly increased compared to the bare sample, signifying a better corrosion inhibition of mild steel in the corrosive environment.

The LDH is also able to perform a 2-way role where it is able to release the nitrate as a corrosion inhibitor to adhere to the metal surface and also entrap the harmful chloride into the metal layers, which reduces the amount of corrosive chloride in the test solution [29].

(a)

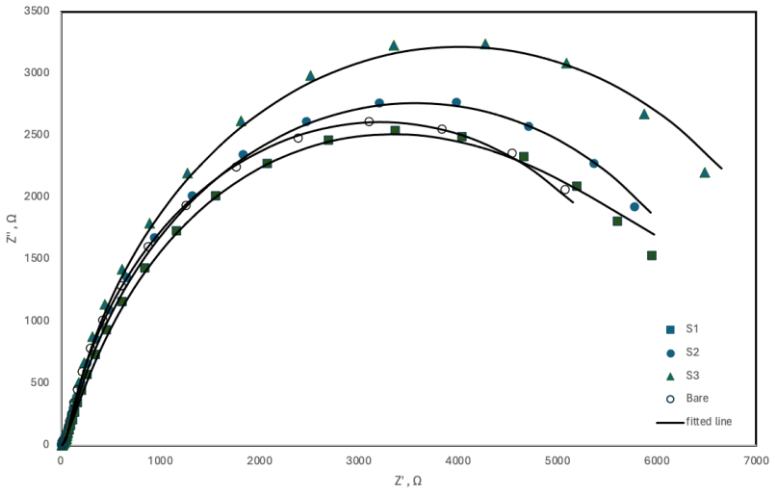

(b)

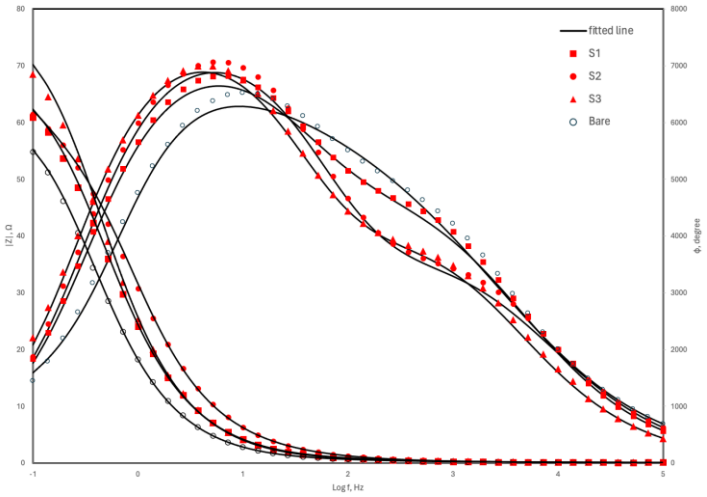

Figure 7 (a) Impedance spectra, and (b) Bode plots of mild steel in neutral 3.5 wt% NaCl solution with, and without the presence of LDH.

The Bode plot in **Figure 7(b)** shows the impedance modulus of S3 is the highest signifies the improvement in the corrosion inhibition as compared to the test solution without the presence of LDH. High impedance modulus signifies higher ion exchange of nitrate from LDH gallery with chloride in the test solution. Other 2 samples, S1 and S2 show similar impedance modulus signifying almost similar inhibition

efficiency as observed with relatively similar capacitive arcs behavior in the Nyquist plot.

The Bode diagrams for the test solution with LDH were characterized as 2-time constants where the low frequency was attributed to the dissolution of iron, while the higher frequency was attributed to the precipitation of Mg^{2+} onto the mild steel [30]. The shape of the bare solution without the presence of LDH shows a significant different compared to the solution with the presence of LDH. It was observed that all samples show increase in the intensity of the Bode plot with similar pattern, signifying similar inhibition mechanism by the LDH. The magnitude of the Bode plot intensity follows the pattern on capacitive arcs in Nyquist plot where S3 is the highest, followed by S2 and S1.

The polarization curves displayed in **Figure 8** was carried out to investigate the anticorrosion potential of LDH introduced in the 3.5 wt% NaCl solution. The corrosion potential (E_{corr}), current density (I_{corr}), and inhibition efficiency (η) were calculated and tabulated in **Table 4**.

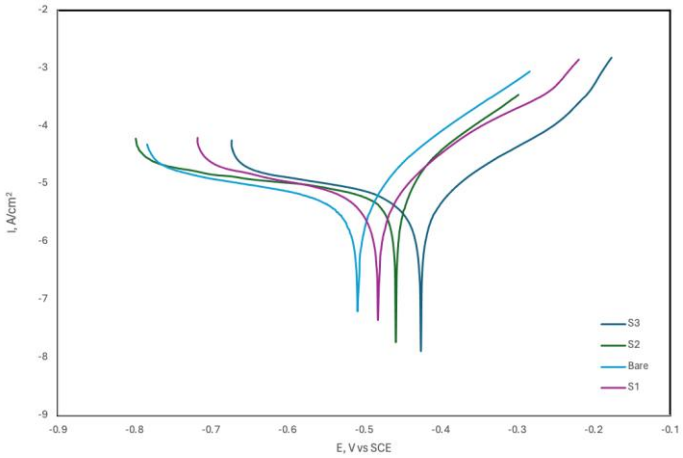

Figure 8 Potentiodynamic polarization curves for mild steel in 3.5 wt% NaCl solution with, and without LDH.

The shift of corrosion potential value towards more positive value indicates the increase in corrosion resistance of mild steel in the corrosive media. The corrosion current values also reduced significantly on S3 where the cathodic curve is observed to be decreased. The anodic curves are observed at slightly higher magnitude as the metal concentration increased indicating the LDH particle with positive charged adsorbed at the anodic site [15].

The cathodic protection was observed from the significant difference in the magnitude of the cathodic curves. These observations make clear that the corrosion inhibition is majorly contributed by the cathodic protection reaction from the nitrate released from the LDH structure. The release of nitrate from the LDH structure was due to the ion exchange with the aggressive chloride that was the main contributor to the corrosion of mild steel. Additionally, the Mg^{2+} from the LDH layer is also able to form a precipitate of magnesium hydroxide at the cathodic sites to further reduce the cathodic current densities.

Table 4 Fitted parameters from polarization data obtained for 3.5 wt% NaCl solution with and without LDH.

	E_{corr}, V_{SCE}	I_{corr}, μA/cm²	η, %
Bare	–0.50716	86.925	-
S1	–0.48304	78.729	9.43
S2	–0.45951	76.717	11.74
S3	–0.42732	9.886	88.63

The corrosion current values were observed to be decreasing with the increase in the metal concentration. Lower corrosion current signifies higher corrosion protection and vice versa [26]. The corrosion inhibition efficiency of S1 and S2 are within the expected range, relatively close as discussed based on Nyquist and Bode plots by the findings of the capacitive arcs and Bode intensity, respectively. S3 with the highest nitrate amount has the highest corrosion inhibition of 88.63% compared to the test solution without LDH. This result shows that the presence of interferences of metal oxides observed from PXRD patterns does not affect the ability of LDH to perform the ion exchange process.

Conclusions

This study reveals that the concentration of the metals used to form the LDH structure contributes to the LDH characteristics of the final product, which primarily affects the amount of anion loading. High concentration of metal used in S3 resulted with the highest nitrate loading with 2.33% compared to lower nitrate loading in S1 and S2 with 1.06% and 1.29%, respectively. It was also observed that higher metal concentration formed impurities such as AlOOH and $MgCO_3$ in the PXRD patterns of S2 and S3 due to incomplete reaction. The thermal behaviors of the samples revealed different trends, concurrent with PXRD data. The presence of interferences observed in samples S2 and S3 did not limit the ability of LDH structure to perform the unique anion exchange when tested in the corrosive media for mild steel protection. S3, with the highest nitrate amount, observed with 88.63% corrosion inhibition compared to others. This shows that the LDH is still able to perform the ion exchange process with the presence of interferences, such as the metal oxides, due to the incomplete reaction.

Acknowledgements

The authors gratefully acknowledge the financial support provided by the Journal Support Fund from Universiti Teknologi MARA (UiTM), Malaysia and Institute of Postgraduate Studies UiTM, Malaysia for the publication of this article.

Declaration of Generative AI in Scientific Writing

The authors acknowledge the use of generative artificial intelligence (AI) tools to assist in the preparation of this manuscript. AI was employed to support language refinement, improve readability, and suggest alternative phrasing of the text. However, all research design, data collection, analysis, interpretation, and final conclusion are the sole work of the authors. The authors have thoroughly reviewed, edited, and approved the entire manuscript to ensure accuracy, originality, and academic integrity.

CRediT Author Statement

Mohamad Nor Amirul Azhar Kamis: Investigation, Methodology, Data curation, Writing-original draft, Writing-review & editing. **Hamizah Mohd Zaki:** Project administration, Funding acquisition, Supervision, Validation, Writing-review & editing. **Adila Mohamad Jaafar:** Validation. **Mohammad Noor Jalil:** Validation. **Nur Shafiqa Nabila Mohd Nor:** Investigation, Methodology.

References

[1] J Kameliya, A Verma, P Dutta, C Arora, S Vyas and RS Varma. Layered double hydroxide materials: A review on their preparation, characterization, and applications. *Inorganics* 2023; **11(3)**, 121.

[2] CM Terzi, ED Santos, C Carvalho, V Prevot, F Wypych, C Forano and S Nakagaki. MgAl and ZnAl layered double hydroxides modified with molybdate and tungstate anions as catalysts for oxidation of cyclohexane. *Catalysis Today* 2023; **422(281)**, 114221.

[3] Y Gu, Z Yang, J Zhou, Q Fang, X Tan and Q Long. Graphene/LDHs hybrid composites synthesis and application in environmental protection. *Separation and Purification Technology* 2024; **328**, 125042.

[4] AM Cardinale, C Carbone, S Molinari, G Salviulo and F Ardini. MgAl-NO_3 LDH: Adsorption isotherms and multivariate optimization for Cr (VI) removal. *Chemistry* 2023; ***5*(1)**, 633-645.

[5] C Jing, B Dong, A Raza, T Zhang and Y Zhang. Corrosion inhibition of layered double hydroxides for metal-based systems. *Nano Materials Science* 2021; **3(1)**, 47-67.

[6] AM Lauermannová, I Paterová, J Patera, K Skrbek, O Jankovský and V Bartůněk. Hydrotalcites in construction materials. *Applied Sciences* 2020; **10(22)**, 7989.

[7] I Imanieh and A Afshar. Synthesis parameters effect on the final morphology of the layered double hydroxide (LDH). *Protection of Metals and Physical Chemistry of Surfaces* 2017; **53(3)**, 460-465.

[8] HS Panda, R Srivastava and D Bahadur. Synthesis and in situ mechanism of nuclei growth of layered double hydroxides. *Bulletin of Materials Science* 2011; **34(7)**, 1599-1604.

[9] MNAA Kamis, H Mohd Zaki, Z Mohd Zain, MN Jalil and ME Khairul Azly. Optimizing corrosion resistance: How pH shapes the inhibition mechanism of ZnAl-NO_3^-LDH on mild steel. *Pure and Applied Chemistry* 2025; **97(4)**, 381-399.

[10] Y Cao, D Zheng, S Dong, F Zhang, J Lin, C Wang and C Lin. A composite corrosion inhibitor of MgAl layered double hydroxides co-intercalated with hydroxide and organic anions for carbon steel in simulated carbonated concrete pore solutions. *Journal of The Electrochemical Society* 2019; **166(11)**, C3106.

[11] Y Zhang, S Li, B Qiu, S Chen, H Chen and X Fan. MgAl layered double hydroxide (LDH) for promoting ammonia synthesis in non-thermal plasma: Role of surface oxygen vacancy. *Chemical Engineering and Processing - Process Intensification* 2024; **195**, 109608.

[12] R Trujillano. 30 years of Vicente Rives' contribution to hydrotalcites, synthesis, characterization, applications, and innovation. *ChemEngineering* 2022; **6(4)**, 60.

[13] C Ramajeya and K Balasubramanian. Multifaceted analysis of L-alanine-doped Creatininium benzene sulphonate single crystals for optical modulation application. *Journal of Environmental Nanotechnology* 2024; **13(3)**, 374-384.

[14] T Hibino. Anion selectivity of layered double hydroxides: Effects of crystallinity and charge density. *European Journal of Inorganic Chemistry* 2018; **2018(6)**, 722-730.

[15] TD Nguyen, BA Tran, KO Vu, AS Nguyen, AT Trinh, GV Pham, TXH To, MV Phan and TT Phan. Corrosion protection of carbon steel using hydrotalcite/graphene oxide nanohybrid. *Journal of Coatings Technology and Research* 2019; **16**, 585-595.

[16] B Habibi, A Pashazadeh, S Pashazadeh and LA Saghatforoush. A new method for the preparation of MgAl layered double hydroxide-copper metal–organic frameworks structures: Application to electrocatalytic oxidation of formaldehyde. *Scientific Reports* 2024; **14(1)**, 5222.

[17] JY Yap, SM Yaakob, NE Rabat, MR Shamsuddin and Z Man. Release kinetics study and anti-corrosion behaviour of a pH-responsive ionic liquid-loaded halloysite nanotube-doped epoxy coating. *RSC Advances* 2020; **10(22)**, 13174-13184.

[18] A Misol, FM Labajos, A Morato and V Rives. Synthesis of Zn, Al layered double hydroxides in the presence of amines. *Applied Clay Science* 2020; **189**, 105539.

[19] M Khitous, Z Salem and D Halliche. Removal of phosphate from industrial wastewater using uncalcined MgAl-NO_3 layered double hydroxide: batch study and modeling. *Desalination and Water Treatment* 2016; **57(34)**, 15920-15931.

[20] J Zuo, B Wu, C Luo, B Dong and F Xing. Preparation of MgAl layered double hydroxides intercalated with nitrite ions and corrosion protection of steel bars in simulated carbonated concrete pore solution. *Corrosion Science* 2019; **152(7)**, 120-129.

[21] SK Poznyak, J Tedim, LM Rodrigues, AN Salak, ML Zheludkevich, LFP Dick and MGS Ferreira. Novel inorganic host layered double hydroxides intercalated with guest organic inhibitors for anticorrosion applications. *ACS Applied Materials & Interfaces* 2009; **1(10)**, 2353-2362.

[22] ML Jadam, SAS Mohamad, HM Zaki, Z Jubri and SH Sarijo. Antibacterial activity and physicochemical characterization of calcium-aluminium-ciprofloxacin-layered double hydroxide. *Journal of Drug Delivery Science and Technology* 2021; **62(3)**, 102314.

[23] SNM Sharif, N Hashim, IM Isa, SA Bakar, MI Saidin, MS Ahmad, M Mamat, MZ Hussein and R Zainul. Polymeric nanocomposite-based herbicide of carboxymethyl cellulose coated-

zinc/aluminium layered double hydroxide-quinclorac: A controlled release purpose for agrochemicals. *Journal of Polymers and the Environment* 2021; **29(6)**, 1817-1834.

[24] S Li, Y Shen, M Xiao, D Liu and L Fan. Synthesis and controlled release properties of *β*-naphthoxyacetic acid intercalated Mg-Al layered double hydroxides nanohybrids. *Arabian Journal of Chemistry* 2019; **12(8)**, 2563-2571.

[25] Z Jiang, J Wu, X Liu, H Yu, C Jiao, J Shen and Y Pei. Facile synthesis of MgAl layered double hydroxides by a co-precipitation method for efficient nitrate removal from water: Kinetics and mechanisms. *New Journal of Chemistry* 2021; **45(32)**, 14580-14588.

[26] SH Adsul, UD Bagale, SH Sonawane and R Subasri. Release rate kinetics of corrosion inhibitor loaded halloysite nanotube-based anticorrosion coatings on magnesium alloy AZ91D. *Journal of Magnesium and Alloys* 2021; **9(1)**, 202-215.

[27] ZB Jubri, NZABM Yusoff, SHB Sarijo, ESB Marsom and MZB Hussein. Synthesis, characterization and controlled release properties of zinc–aluminium-beta-naphthoxyacetate nanocomposite. *Journal of Porous Materials* 2017; **24(3)**, 573-582.

[28] RC Zeng, ZG Liu, F Zhang, SQ Li, HZ Cui and EH Han. Corrosion of molybdate intercalated hydrotalcite coating on AZ31 Mg alloy. *Journal of Materials Chemistry A* 2014; **2(32)**, 13049-13057.

[29] W Li, A Liu, H Tian and D Wang. Controlled release of nitrate and molybdate intercalated in Zn-Al-layered double hydroxide nanocontainers towards marine anticorrosion applications. *Colloid and Interface Science Communications* 2018; **24**, 18-23.

[30] GJ Ayemi, S Marcelin, S Therias, F Leroux and B Normand. Synergy effect between layer double hydroxide (LDH) and EDDS for corrosion inhibition of carbon steel. *Applied Clay Science* 2022; **222**, 106497.